

Integrating Soft Robotics: The Design, Fabrication, and Control of a Pneumatic Gripper

Guanyu Xu, *UM-SJTU JI*, Jiawen Li, *UM-SJTU JI*, Weixuan Zhang, and Youle Chen, *UM-SJTU JI*

Abstract—Soft robotics is an emerging field with promising applications in delicate tasks such as medical operations, disaster response, and agricultural activities, where the handling of soft and deformable objects is required. This study addresses the need for a versatile soft gripper, integrating with a precise control system. Our goal was to create a soft pneumatic gripper within a crane-like system for basic manipulation tasks, challenging for rigid grippers. We designed a four-finger pneumatic soft gripper and a robotic arm with four degrees of freedom. The gripper, featuring elastomeric fingers with interconnected air chambers, prioritized adaptability and ease of manufacturing. The robotic arm, equipped with rotational and lifting mechanisms driven by motors, ensured the required range of motion. Control was managed via Arduino and Bluetooth modules, facilitating wireless operation through a custom mobile app. We successfully designed and fabricated the gripper and arm, demonstrating their ability to handle objects of varying shapes and sizes safely. The system's stability and safety were validated through theoretical analysis and experimental testing. Meeting expectations, our system shows promise for broader applications in fields like biology, medicine, and disaster relief. This work advances soft robotics by offering a practical, cost-effective solution for manipulating delicate objects with precision and adaptability.

Index Terms—Soft robotics, Pneumatic gripper, Control system, Design and manufacturing

I. INTRODUCTION

SOFT robotics has emerged as a promising area with a wide range of potential uses in medical fields, disaster response, and agricultural tasks such as crop harvesting and handling [1] [2]. Furthermore, while conventional rigid grippers with joints and links demand high mechanical and control complexity to attain the necessary speed, flexibility, and dexterity for manipulating soft and deformable objects [3], soft grippers can easily meet these objectives by adapting to the object's shape and evenly distributing grasping forces [4] [5]. Meanwhile, the evaluation of gripping performances [6] as well as the combination of the gripper and other control systems, such as robotic arms, remain to be investigated. Therefore, the problem we are interested in is that we need to design and manufacture a soft gripper to grasp various types of objects, including convex, non-convex, and flat, and use a control system to realize simple manipulation, performing tasks such as pouring water from a bottle.

Guanyu Xu is the main leader of the team, who is responsible for the overall design of the system as well as the manufacturing process. This project is impossible to complete without him.

Jiawen Li mainly helps the design review presentation as well as the final project with his technical communication skills. He is also responsible for the theoretical analysis of the system.

Weixuan Zhang and **Youle Chen** also devotes countless efforts to this project, especially in the manufacturing process. It is the joint effort of the whole team that makes this project possible.

Recent years have witnessed numerous designs of soft grippers (Table I). Brown et al. [7] proposed a universal soft gripper with a single mass of granular material that utilizes the evacuation of air to achieve rigidity when picking and putting the objects. However, such a gripper has a size limit for the object and is unable to grasp flat or deformable objects [3]. W. Zheng et al. [8] suggest a soft bending actuator design that uses a single air chamber and fiber reinforcements with simulation analysis. Nevertheless, the fibers add to the difficulty of manufacturing and its real application performance remains to be tested. Another kind of mature approach is to use soft pneumatic actuators, or FEAs (Fluidic Elastomer Actuators). They have several advantages including adaptability, easy fabrication, robustness, and low-cost elastomer materials despite not suitable for heavy objects [9], [10]. Ilievsk et al. [11] suggested a three-layer gripper design utilizing PneuNets, which are attached as a whole with bending FEAs produced through soft lithography. Then, Mosadegh et al. [12] proposed rapidly actuating PneuNets with independent control and showed its fast speed, larger force, and higher durability. However, Mosadegh et al. do not perform tests on gripping effectiveness of such a design. Later Y. Hao et al. [13] suggested a four-finger pneumatic elastomeric robot, mimicking biological fingers with experiments showing its satisfactory grasping performance. Therefore, pneumatic soft grippers with independent fingers are prospective and could be adopted.

Our work proposes a four-finger pneumatic soft gripper design combined with a crane-like control system with 4 DoF to grasp and move different kinds of objects in a certain area. The main robotic arm can rotate, lift, and make the gripper move forward and backward. The pneumatic soft gripper is attached to an air pump and can be controlled to grasp, release, and rotate. In addition, our work discusses the detailed manufacturing process of the soft gripper and gives a thorough test and analysis of the performance of the whole system with experiments.

II. DESIGN

A. Design of the Soft Gripper

The soft gripper (Fig. 1) mainly consists of three components: 1). Four soft elastomeric fingers. 2). A cross-shaped fixator with four fixing holes. 3). A U-shaped connector. Each pneumatic soft elastomeric finger comprises ten interconnected air chambers. When inflated with air, the fingers bend and provide grasping force to the object. The four fingers are fixed in the correct configuration using a cross-shaped fixator.

No.	Method	Major Findings	Unresolved Issues	Refs.
L1	Universal soft gripper with granular material	Evacuation of air achieves rigidity for object manipulation	Size limit for objects, inability to grasp flat or deformable objects	[7]
L2	Soft bending actuator with single air chamber and fiber reinforcements	Modelling and simulating the force of soft bending actuator	Difficulty in manufacturing due to added fibers, no real-life test	[8]
L3	Soft pneumatic actuators (FEAs)	Adaptability, easy fabrication, robustness, low-cost materials	limited forces, vulnerable to damages	[9], [10]
L4	Three-layer gripper design utilizing PneuNets	Utilizes bending FEAs produced through soft lithography	Not suitable for heavy objects,	[11]
L5	Rapidly actuating PneuNets with independent control	Fast speed, larger force, higher durability	Grasping performance not tested	[12]
L6	Four-finger pneumatic elastomeric robot	Mimics biological fingers, satisfactory grasping performance	lack of a control system	[13]
L7	Proposed Work	Two configurations of gripper with inflation and deflation	Lack of detailed analysis on grasping force	-

TABLE I: Literature review of soft grippers

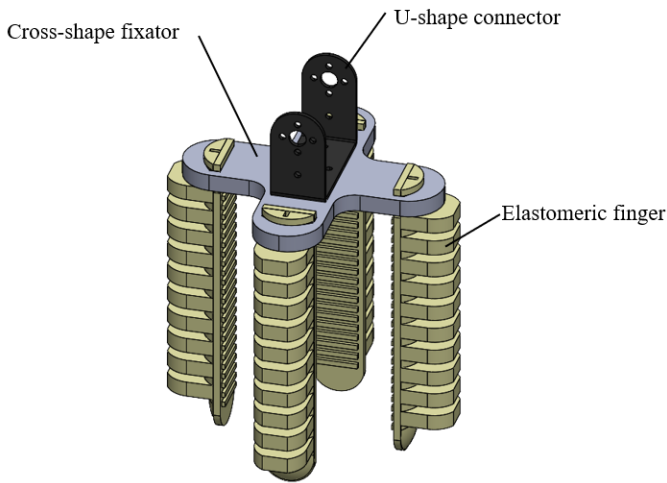


Fig. 1: The overall design of the soft gripper.

Finally, a U-shaped connector is used to attach the gripper to the robotic arm. To inflate the fingers with air, four separate tubes need to be inserted into the finger through the hole at the top end.

Compared to other similar designs, the main difference of our gripper is that it consists of four separate fingers. This feature is advantageous in terms of three aspects: more adaptable configuration, convenience in reparation, and economy in manufacturing.

1) *Adaptable configuration:* The design of separate fingers allows the gripper to have a bidirectional bending: bend inward when inflated, and bend outward when deflated [13]. This leads to two possible configurations of the gripper concerning the orientation of elastomeric fingers (Fig. 2). In the inflation configuration, the four fingers are fixed so that the chamber side is pointing outward. In this case, the gripper will close when inflated (chamber air pressure is greater than outside pressure). On the other hand, for the deflation configuration, the four fingers are fixed so that the chamber is pointing

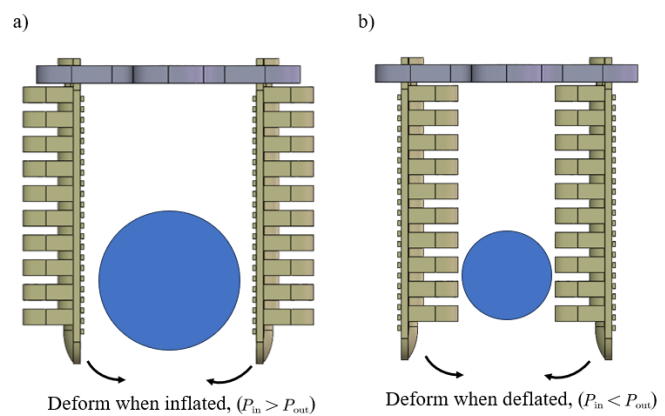


Fig. 2: Two configurations of the gripper concerning the orientation of the fingers. a). The inflation configuration, b). The deflation configuration.

inward. In this case, the gripper will close when deflated (chamber air pressure is smaller than air pressure). Ideally, in the deflation configuration, the maximum bending capacity is relatively smaller than the inflation configuration, and so is the grasping force it can provide. Therefore, we choose to use the inflation configuration in our final project.

2) *Convenience in reparation:* This design also ensures independence between various parts of the gripper. Compared with the cross-shaped design, if air leakage is detected in one of these fingers, we only need to repair or replace the broken part, which greatly saves the materials needed for the gripper. In addition, daily maintenance is convenient since it is easy to disassemble and assemble, thus avoiding casual damage to other parts.

3) *Economy in manufacturing:* The design of four separate fingers is more economical than four connected fingers in the 3D printing process. Ideally, we only need to print one base mode to make all four fingers, which consumes much less 3D printing material than producing a mold for a connected gripper. Besides, during the testing process, We can estimate

the actual effect of the whole gripper based on the performance of one finger. If we find that the finger design has quality issues and fails to meet functional requirements, we only need to process a new one based on the improved design, which greatly saves materials and time.

B. Design of the Crane-like Robotic Arm

A crane-like robotic arm system with 4 degrees of freedom is designed to enable the gripper to reach every point within a cylinder 1 meter in diameter and 20 centimeters in height. The overall design is shown in Fig. 3.

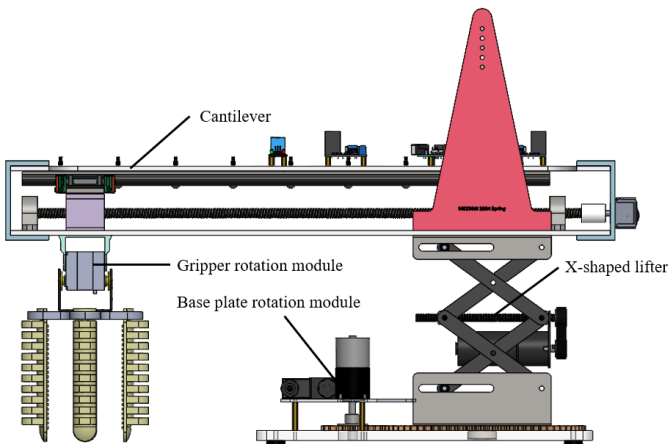


Fig. 3: The CAD drawing of the whole system with each subsystem labeled: The *Cantilever* is the horizontal block that is used for the radial movement of the gripper. The *Gripper Rotation Module* is fixed on to the top of the gripper. The *Base Plate Module* consists of two meshed gears, and the *X-Shaped Lifter* drives the vertical movement which is align with the rotational axis.

1) Base Plate Module: The details of the base plate rotation module are shown in Fig. 4. It mainly consists of two meshed gears of different sizes, bearings, a flange and a DC motor (6GM-3530, DC12V, 1540RPM). The big gear, small gear, and two plates in the base plate rotation module are made of acrylic (polymethyl methacrylate, PMMA), and are manufactured by laser cutting. The main function of the gear transmission structure is to separate the axis of rotation and the axis of the motor to provide enough space for the base plate rotation motor. After determining the dimensions, the two meshed gears are fixed to the base plate through bearings and shafts. A DC motor is connected to the small gear through a flange to provide power for the system. When the motor is turned on, the small gear starts to rotate, and the torque is transmitted to the large one, driving the structure on the gear to rotate around the central axis of the large gear.

The creativity in the design of this module includes cleverly utilizing the relationship of torque and power in gear transmission. The system converts low torque at high speeds into high torque at low speeds, thereby driving heavy objects to rotate freely at low speeds on a horizontal plane. In addition, the shaft connecting the bearing and the base plate is designed as a concentric configuration, which means that the hole in

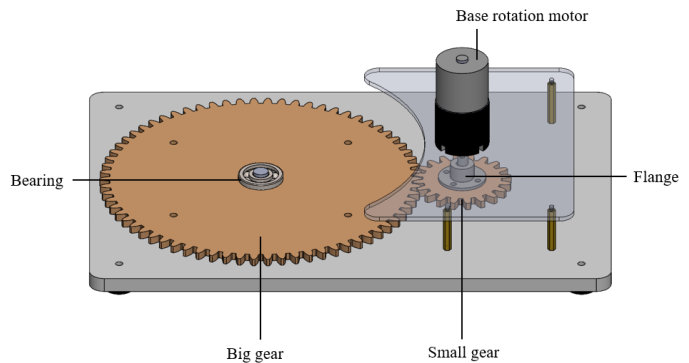


Fig. 4: Detailed CAD drawing of the base plate rotation module.

the center of the shaft can facilitate wire connection for the mechatronic system.

2) X-shaped Lifter: The detail of the X-shaped lifter is shown in Fig. 5. It mainly consists of top connectors, bottom connectors, gears, synchronous belt, two power screws and a DC motor(36GM-36ZY, DC12V, 570RPM). Most parts (excluding a synchronous belt) are made of metal (steel or aluminum alloy). The main structure of the lifter are eight scissor rods (four on each side), which are used to support the entire weight of the upper structure while guaranteeing the vertical movement. The scissor rods are made of aluminum alloy and are manufactured by laser cutting. Top and bottom connectors are made of steel, which are made into L-shape by sheet metalworking.

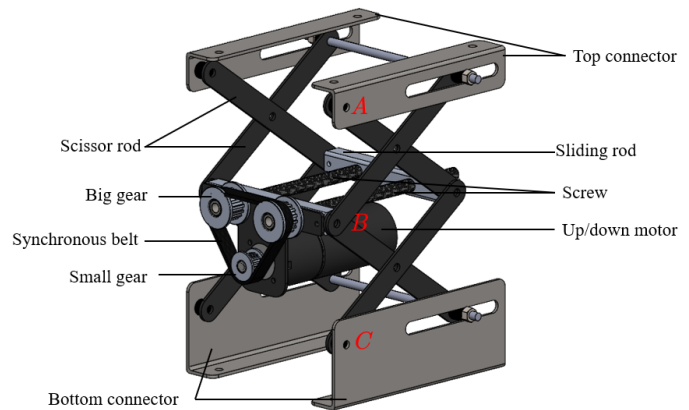


Fig. 5: Detail CAD drawing of the X-shaped lifter.

When the motor is turned on, it drives the small gear and brings the two large gears into rotation through the belt transmission, and finally causes the screws to rotate. Then, the screws transform the rotation motion into horizontal motion, thereby driving the sliding rod to move left or right. When the distance between the left and right ends of the X-shape changes, the height changes accordingly, thus realizing controllable lifting and lowering.

The creativity in the design of the X-shaped lifter includes clever positioning of the motor and two screws that are partially threaded. Firstly, the motors are rigidly connected to the *B* end of the scissor rod (Fig. 5), ensuring that the

vertical position of the motor won't change relative to the screw during the lifting and lowering process. Secondly, only part of the screw has thread (at *B* end, the screw doesn't have thread), which means that when the lifer moves up or down, points *A*, *B*, and *C* will always stay on the same vertical line. This will guarantee that the horizontal position of the motor won't change as well.

The X-shaped lifter also takes advantage of the power and torque relation within the belt and gear transmission. A small gear is directly connected to the output axis of the motor, and power is transmitted through a synchronous belt to two large gears, with torque amplified. Two power screws run parallel to each other to double the force acting on the sliding rod.

3) *Cantilever*: The detail of the cantilever is shown in Fig. 6. It mainly consists of two acrylic boards, the guide track, a linear screw, a sliding block, two bearings and a DC motor (4632-370, DC12V, 150RPM). The core of the design is using power screw to convert rotational motion from the motor into linear motion. A guide track is added to balance the sliding block. First, the guide track is fixed to the top board. Then, the sliding block is nested into the guide track. The screw passes through the center of the sliding block, and is fixed to the bottom board by two journal bearings. One end of the screw is connected to the DC motor. When the motor is powered on, the screw begins to rotate, and it converts torque into axial force, thereby driving the slider to move horizontally. The movement direction of the slider can be reversed by changing the rotation direction of the motor. Besides, the sliding block is fixed to the guide track to avoid vertical rotation around the screw.

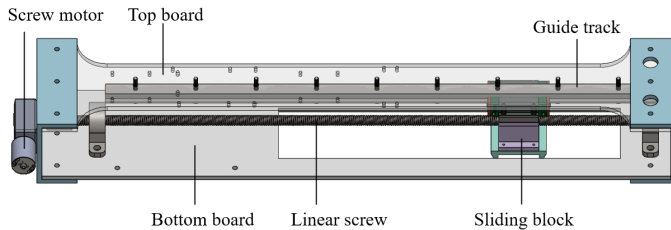


Fig. 6: Detailed CAD drawing of the Cantilever.

The working principle of the linear screws is creatively utilized in the design, enabling free horizontal movement of the slider through the simplicity and reversibility of screw transmission.

4) *Gripper Rotation Module*: The detail of the gripper rotation module is shown in Fig. 7. It mainly consists of a screw block, a U-shaped bracket, a gripper connector, a cross-shaped fixator and a servo motor (Double Axis, 10Kg, DC6V). The gripper connector is fixed to the screw block so that the gripper is able to move alongside the sliding block in a horizontal direction. The U-shaped bracket is used to connect the servo with the cross-shaped fixator. When the servo motor is powered on, it will drive the claw to rotate vertically.

The design controls the vertical rotation of the claw through the working principle of the servo, using brackets and connectors to ensure the stability of the power transmission in different directions.

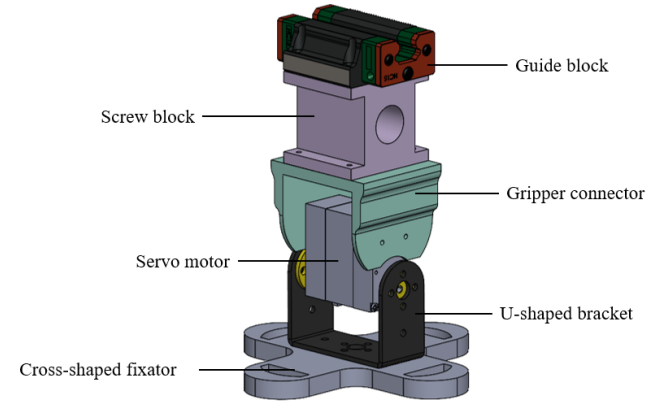


Fig. 7: Detailed CAD drawing of the gripper rotation module.

III. MANUFACTURING

A. Justification of Selection of Materials

Different kinds of materials are selected for different parts of the robotic arm and soft gripper to optimize the weight, provide enough strength, and fulfill their desired functionality. Two major parts that require careful justification for the selection of materials are

- The **top board** and **bottom board** of the *Cantilever* structure, which are required to be light and stiff panels.
- The **scissor rods** of the *X-shaped lifter* structure, which is required to be light and stiff tie.

1) *Light, stiff panel*: Panel structures, mainly including the top board and bottom board in the cantilever, etc., are widely used in the design of the robotic arm due to their simplicity in modeling and convenience in actual manufacturing. To optimize the design, we want these panels to be light and stiff. Specifically, these structures will usually be loaded in bending by a given force F (Fig. 8). To guarantee the proper functionality, we want to restrict the deflection of these structures under a given value δ . The objective is to achieve this within a minimum mass m .

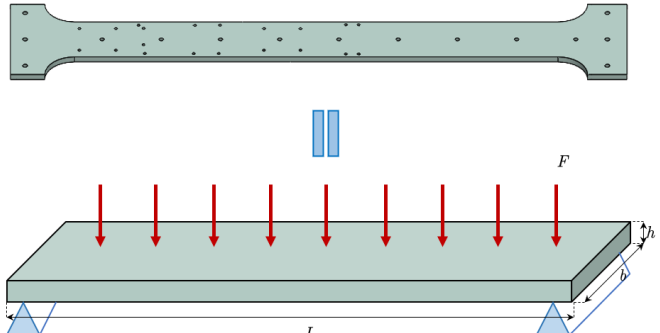


Fig. 8: The model of the *top board* in the Cantilever, simplified as a panel loaded in bending by a uniformly distributed force F .

Let b be the width, h be the thickness, and L be the length of a panel (the difference in cross-sectional area is ignored

in the material selection process), and ρ be its density. The objective function can be written as

$$m = \rho b h L$$

To constrain the deflection, the bending stiffness S must be at least S^* , i.e.,

$$S = \frac{C_1 EI}{L^3} \geq S^*$$

where C_1 is a constant determined by the loading, and I is the moment of inertia of the cross-section, which is given by

$$I = \frac{1}{12} b h^3$$

Plug in all these quantities, we can rewrite the objective function as

$$m = \left(\frac{12S^*}{C_1 b} \right)^{1/3} b L^2 \left(\frac{\rho}{E^{1/3}} \right) \quad (1)$$

In equation 1, the last term $\frac{\rho}{E^{1/3}}$ is determined by the property of the material. Thus, we can use an Ashby chart [14] with Young's modulus E plotted against material density ρ (Fig.9) to select material along the guideline of $\frac{E^{1/3}}{\rho}$.

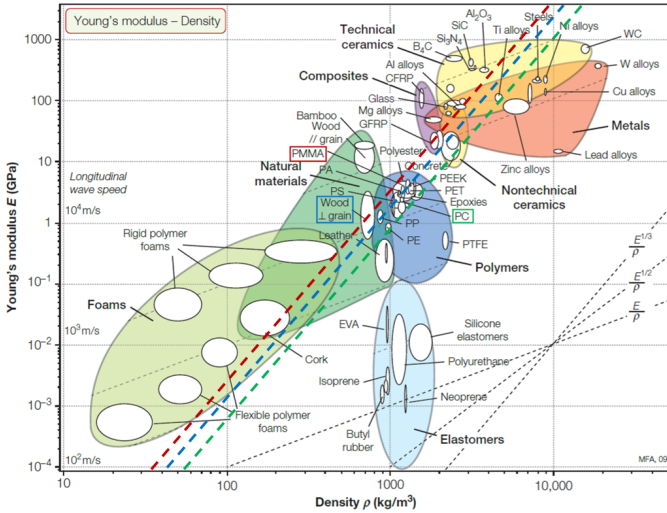


Fig. 9: Ashby chart with Young's modulus plotted against density ρ . The guideline $\frac{E^{1/3}}{\rho}$ is used for the design of a light, stiff panel.

Taking into account the convenience in the manufacturing process of these panels, the candidate materials for these panels are polymethyl methacrylate (PMMA), wood (\perp to grain), and polycarbonate polymer (PC). In Fig. 9, three dashed lines with different colors are drawn parallel to the $\frac{E^{1/3}}{\rho}$ guideline to represent different materials. The red line represents PMMA, the blue line represents wood, and the green line represents PC. Therefore, we know the best option for the beam structures is PMMA.

2) *Light, stiff tie*: Tie structure, mainly referring to the scissor rods in the X-shaped lifter, should be light and stiff as well. Specifically, these members will generally be loaded in compression with a given force F (Fig.10). To guarantee the proper functionality of these rods, we want to constrain

the axial displacement under a specific value δ . The objective is also to minimize mass m .

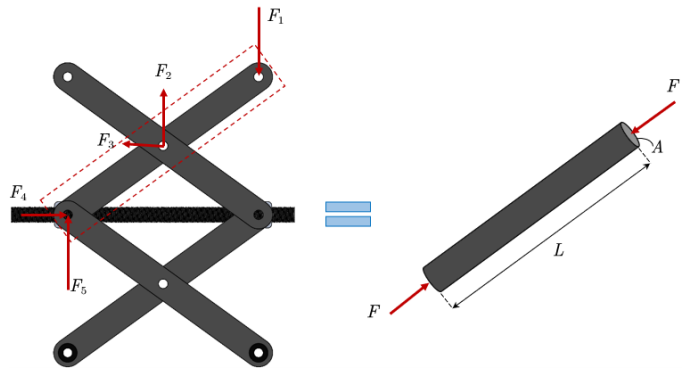


Fig. 10: The model of the *scissor rod* in the X-shaped lifter, simplified as an axially loaded rod.

Let L be the length, A be the cross-sectional area of the rod, and ρ be the density of its material. The objective function can be written as

$$m = \rho A L$$

To constrain the displacement, the bending stiffness k must be at least k^* , i.e.,

$$k = \frac{EA}{L} \geq k^*$$

Replace the free variable A in the objective function, we can rewrite it as

$$m = k^* L^2 \left(\frac{\rho}{E} \right) \quad (2)$$

The last term in equation 2, ρ/E , is determined by material property, and the $k^* L^2$ term is determined by function and geometry constraints. Therefore, to minimize m , we just need to maximize E/ρ . We will take advantage of an Ashby chart with Young's modulus E plotted against density ρ (Fig. 11), and use guideline E/ρ to select material.

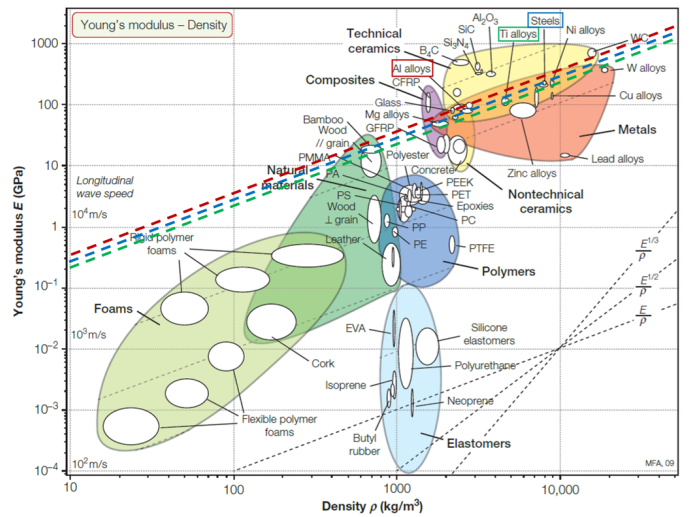


Fig. 11: Ashby chart with Young's modulus E plotted against density ρ . The guideline $\frac{E}{\rho}$ is used for the design of a light, stiff, tie.

The candidate materials for the tie structure are aluminum alloy, titanium alloy, and steel. In figure 11, three dashed lines with different colors are drawn parallel to the guideline E/ρ to represent the candidate materials. The red line represents aluminum alloy, the blue line represents steel, and the green line represents titanium alloy. Therefore, we know the best material for the scissor rod in the X-shaped lifter is aluminum alloy.

B. Justification of Selection of Motors

In this whole system, we use 4 DC motors and 1 servo motor. Among those, three DC motors are carefully selected for them to function properly, which are the base rotation motor (M_b), horizontal screw motor (M_s), and vertical up/down motor (M_v). Their detailed parameters are listed in Table. II. It can be shown that M_v should provide most torque, followed by M_b , and the smallest torque is provided by M_s . The motors can all function properly under this selection.

Name	Type	n_0 (RPM)	T_s (N · m)	I_0 (A)	I_s (A)
M_b	36GM-3530	1154	0.392	0.13	3
M_v	36GM-36ZY	570	1.568	0.25	7.2
M_s	JGY4632-370	150	0.245	0.06	1.3

TABLE II: The detailed parameters of three important DC motors. In the last four columns, n_0 refers to the no-load speed in RPM, T_s refers to the stall torque, I_0 refers to the no-load current, and I_s refers to the stall current. These quantities are taken from the data sheets of the motors.

C. Justification of Manufacturing Processes

Multiple manufacturing processes are involved in this project, including sheet metalworking, milling, turning, polymer shaping, and so on. These processes are carefully selected to ensure proper functionality of each parts as well as the efficiency of the manufacturing.

1) *Robotic arm:* In the robotic arm, we use different manufacturing processes. The basic principle in the selection of manufacturing process is based on their convenience, price, and availability. For example, we use a laser cutting machine to manufacture the acrylic board, and 3D printing to make brackets, sliding blocks, and other parts that are not flat. These two methods are immediately available, so we design the structure such that most parts can be manufactured through these two methods. Some other parts require milling and turning operations, such as the guide track and power screw. These parts are sent to a factory for manufacturing.

2) *Soft gripper:* The mold casting process is widely used in the manufacturing process of the soft gripper. The fabrication of the elastomeric fingers involves 3D printing the mold parts: base mold, up mold, and up mold, and casting the mold with silica gel. For the 3D printing process, we use the Ultimaker 2+ printer with 0.4mm PLA material. A layer height of 0.2mm is chosen in the printing process to ensure the smoothness of the finger surface as well as minimize the printing time. After the 3D printing of the mold is finished, the placing and demolding processes are carried out. We use the double-component liquid silica gel (1:1 mixture) as the filament of the mold.

Specifically, we first pour liquid silica gel into the base mold to about three-quarters full. Then, we put the upper mold inversely into the base mold to squeeze the silica gel to fill all the gaps between the molds. After that, we wait for the silica gel to solidify and pull out the upper half of the finger. We then seal the air chamber by putting the upper half of the finger onto the lid mold filled with silica gel. Finally, we pull the whole finger out of the lid mold and get one finger (Fig. 12). This process is repeated four times to fabricate four identical fingers. A critical point worth mentioning is that during the whole making process, the base mold and lid mold are reused for making all four fingers. This will to a large extent ensure the geometry of the four fingers is the same so that the bending capacity will be similar when they get inflated.

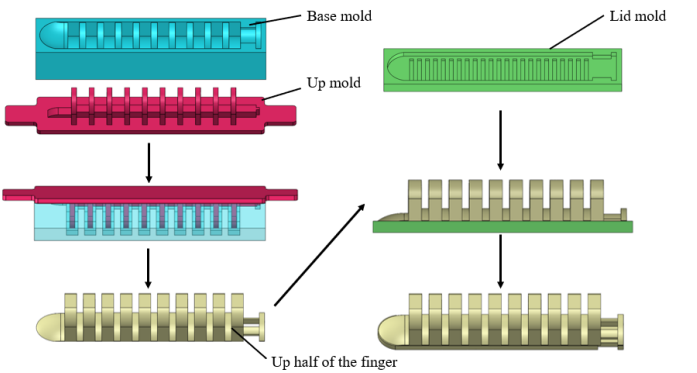


Fig. 12: The process of fabrication one finger

IV. ANALYSIS AND TEST

In the primary design process, only dimensions regarding the shape (e.g., the length and width of the acrylic board) of every part are determined, but those regarding the functionality constraints (e.g. the thickness of the acrylic board) have not been determined yet. We then did some static analysis and testing to determine these parameters. Our goal is to guarantee a factor of safety $F.S. = 3$.

A. Static Analysis on the Cantilever

We are interested in the static characteristics of the bottom board of the cantilever structure because it

- takes most of the weight,
- faces the possibility of breaking.

The thickness d of this board and the mass of the guide track m_g are free variables to be determined. For simplicity, every part is labeled as shown in Fig.13.

First, we draw the free-body diagram of every component in the cantilever structure (Fig. 14). We ignore the weight of two acrylic boards (top board, CD and bottom board, EF), and two 3D-printed brackets, CE and DF . The mass of the power screw, GH , is $m_s = 0.5$ kg. The equilibrium condition of CD yield

$$\sum F_y = F_C + F_D = F_C = F_D = m_g g = 0$$

$$\sum M_C = m_g g \times 320 - F_D \times 640 = 0$$

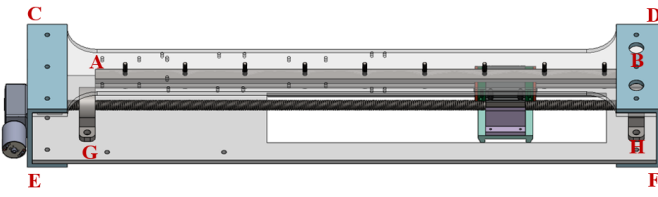


Fig. 13: The labels of each component in the cantilever structure. AB refers to the guide track, CD refers to the top board, EF refers to the bottom board, GH refers to the power screw, and CE and DF refer to the two brackets.

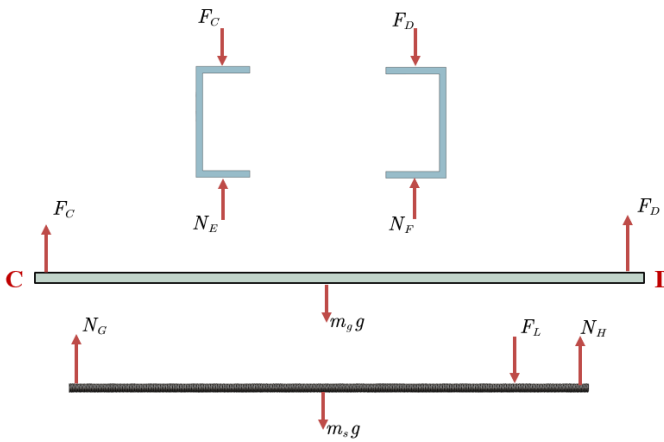


Fig. 14: Free body diagram of each component.

Then, we only consider the condition when the force and moment caused by external load F_L is the maximum, i.e., when the gripper is moved to the outermost position, and the gripper is carrying a maximum weight of $F_L = 5N$. We can write balance equations of screw GH:

$$\begin{aligned}\sum F_y &= N_G + N_F - m_s g - F_L = 0 \\ \sum M_G &= m_s g \times 257.5 + F_L \times 555 - N_F \times 595 = 0\end{aligned}$$

Solving equations, we have:

$$\begin{aligned}N_E &= 1/2m_g g \\ N_F &= 1/2m_g g \\ N_G &= 3.41N \\ N_H &= 6.59N\end{aligned}$$

With those above quantities, we can analyze the bottom board AB. The free body diagram is shown in Fig. 15. By equilibrium condition, we have

$$\begin{aligned}\sum F_y &= \frac{1}{2}m_g g + 3.41 + 6.59 + \frac{1}{2}m_g g \\ &\quad - \frac{1}{2}(w_S + w_N) = 0 \\ \sum M_E &= 3.41 \times 45 - \frac{2}{3}(w_N - w_S) \times 143 - w_S \times 123.5 \\ &\quad + 6.59 \times 595 + \frac{1}{2}m_g g \times 595 = 0\end{aligned}$$

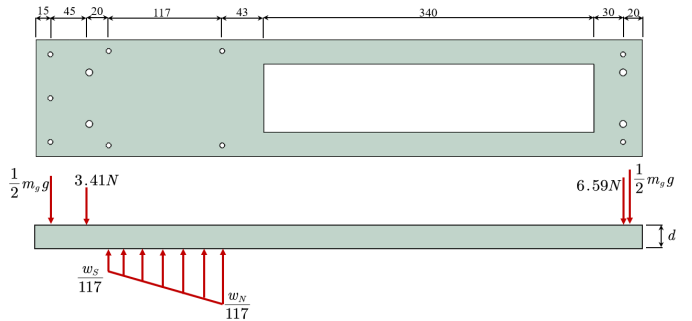


Fig. 15: Free-body diagram of the bottom plate AB, the support by the X-shaped lifter is simplified as a triangle-distributed load.

We can solve for the support w_S and w_N , and get

$$\begin{aligned}w_N &= 52.28 + 25.91m_g N \cdot \text{mm} \\ w_S &= -32.28 - 15.91m_g N \cdot \text{mm}\end{aligned}$$

Before we solve the moment diagram of the board, we can safely assume that the maximum bending moment doesn't occur in between the distributed loading regions. Thus, the distributed loading can be further simplified as a concentrated loading applied at a specific location. Using the method of Macaulay function, we can write out the bending moment M as a function of position x (distance measured from the left end) as

$$\begin{aligned}M &= -5m_g(x - 15) - 3.41(x - 60) \\ &\quad + (-32.28 - 15.91m_g)(x - 123.5) \\ &\quad + (56.37 + 27.88)(x - 143) \\ &\quad + (-6.59 - 5m_g)(x - 595)\end{aligned}$$

Let its derivative be zero, we can get the position of the maximum bending moment, which is $x = 281.7\text{mm}$. At this position, the bending moment is $M = 7887 - 2284m_g N \cdot \text{mm}$ the cross-section of the board is $A = 50d\text{mm}^2$, and its moment of inertial about the neutral axis is

$$I = \frac{1}{12} \cdot (120 - 70) \cdot d^3$$

Then, by the flexure formula, the maximum normal stress in the loaded member is

$$\sigma_{\max} = \frac{Md}{2I} = \frac{7887 - 2284m_g}{2 \times 4.17d^2} \quad (3)$$

The approximate range of m_g and d are $0.5\text{kg} \leq m_g \leq 2\text{kg}$, and $1\text{mm} \leq d \leq 10\text{mm}$. The design plot of σ_{\max} plotted against the mass of the guide track m_g and the thickness of the bottom board d is shown in Fig.16.

Furthermore, we can determine the safety factor by

$$F.S. = \frac{\sigma_f}{\sigma_{\max}} \quad (4)$$

where $\sigma_f = 45\text{MPa}$. The contour plot of safety factor plotted against m_g and d is shown in Fig. 17. In our project, the actual mass of the guide track is $m_g = 1\text{kg}$, from Fig. 17, we can see that to achieve a safety factor of 3, we need the thickness of the bottom board to be about $d = 4\text{mm}$.

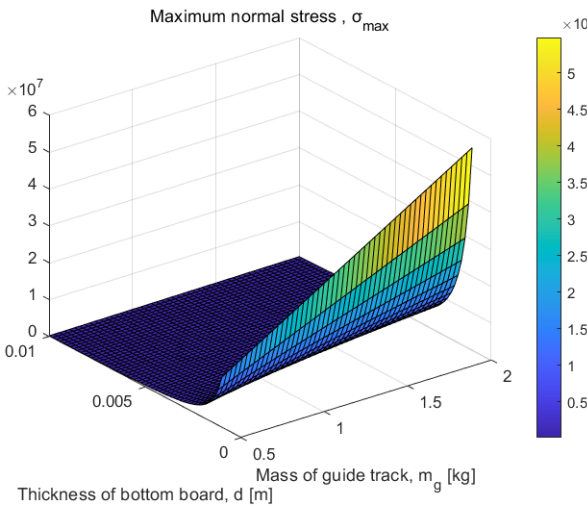


Fig. 16: The design plot of σ_{\max} plotted against m_g and d , according to equation 3.

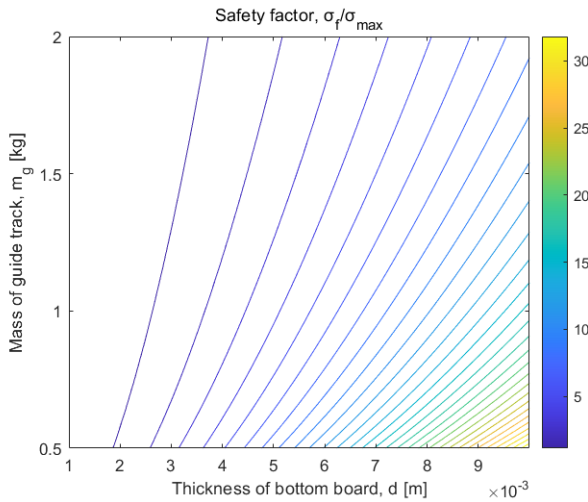


Fig. 17: Contour plot of safety factor plotted against m_g and d , according to equation 4.

To justify the above analytical solution, we conduct a finite element analysis in Solidworks simulation. We add loadings corresponding to $m_g = 1\text{kg}$ at a specific position and set the thickness of the board to $d = 4\text{mm}$. The stress diagram we get from the software is shown in Fig. 18.

From the result, we see that the maximum von Mises stress is about $\sigma = 15\text{MPa}$. The material of this board is acrylic, which has a yielding stress of 45 MPa . The board thickness we choose is 4mm , and we can see that the board will not break down when the loading is 5N , with a factor of safety of 3. This result is aligned with previous analytical solutions.

On the other hand, by running a FEA on the bottom board, we can get the deflection of the board, which is shown in 19. The result shows that there will be relatively large displacement at the tip of the board, which informs us that some ropes are needed to provide balance on the cantilever and to minimize the deflection. The two red triangle brackets in Fig. 3 act as a bracket for the ropes.

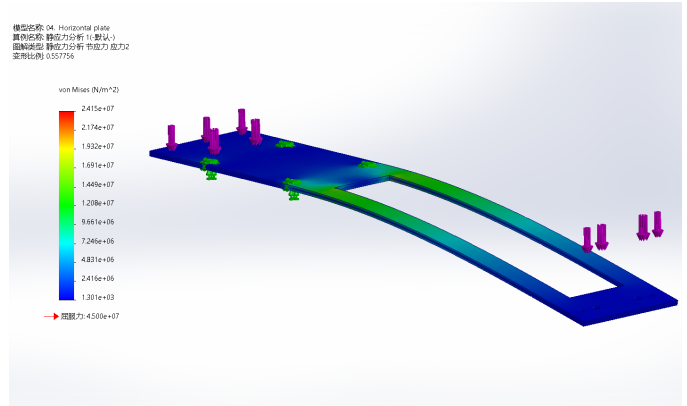


Fig. 18: Finite element analysis result of the von Mises stress distribution on the bottom board.

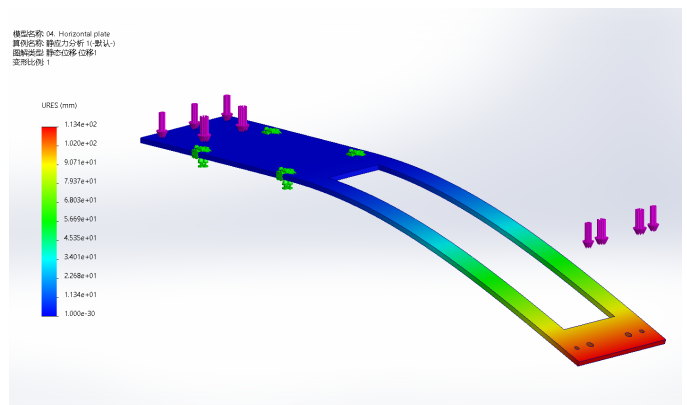


Fig. 19: Finite element analysis result of the URES distribution on the bottom board.

B. Mass Center and the Balance of the Whole System

While the crane-like system is rotating on the base plate, it's important to control the balance of the whole system such that it won't tip over at some position. We will justify this by calculating the mass center of the part that's above the base plate rotation module and analyzing the equilibrium condition. Fig. 20 shows the detailed geometry of the cantilever, X-shaped, and the gripper rotation module. The mass and position of each part are listed in TABLE III.

Name	Mass, [kg]	x , [mm]	y , [mm]
Cantilever	1.7	-176.5	306
X-shaped lifter	2.6	0	138
Gripper	0.8	-416.5	241

TABLE III: The value of mass m and position, x and y coordinates of each part.

The coordinate of the mass center of the upper part is

$$\begin{aligned} x_C &= \frac{\sum x_i m_i}{\sum m_i} \\ &= \frac{1.7 \times (-176.5) + 2.6 \times 0 + 0.8 \times (-416.5)}{1.7 + 2.6 + 0.8} \\ &= -124.2\text{mm} \end{aligned}$$

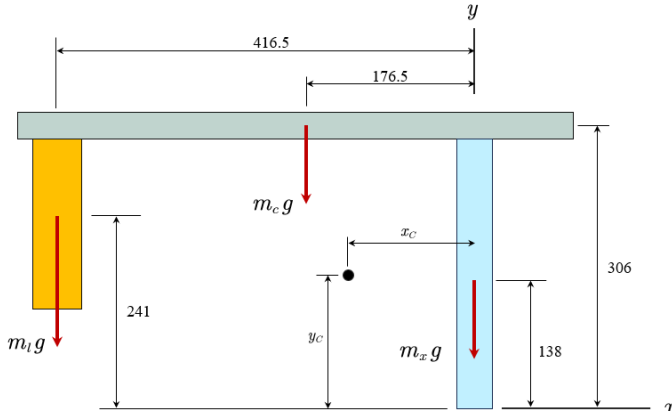


Fig. 20: The detailed geometry of the parts above the base plate rotation module, including the Cantilever (green box), the X-shaped lifter (blue box), and the gripper (orange box).

and,

$$\begin{aligned} y_C &= \frac{\sum y_i m_i}{\sum m_i} \\ &= \frac{1.7 \times 306 + 2.6 \times 138 + 0.8 \times 241}{1.7 + 2.6 + 0.8} \\ &= 210.2 \text{mm} \end{aligned}$$

By inspection, we found that when the cantilever turns to 90° and 180° (Fig. 21), the X-shaped lifter is turned to the highest position, and the gripper is moved to the outermost position, the whole system is most likely to tip over. Thus, we only analysis the equilibrium at these two positions.

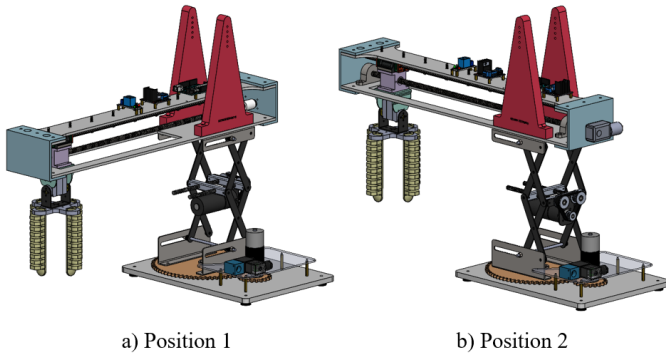


Fig. 21: The position where the cantilever turns to a). 90° , and b). 180°

1) *Position 1:* When the cantilever is turned to 90° position, the free body diagram is shown in Fig. 22. The mass of the base plate rotation module is $m_b = 1.5 \text{kg}$, and $G = (m_c + m_x + m_l)g = 51 \text{N}$. Apply equilibrium equations, we have

$$\begin{aligned} \sum F_y &= N_A + N_B - 51 - 15 = 0 \\ \sum M_A &= 51 \times (125 - 124.2) - N_B \times 250 = 0 \end{aligned}$$

Solve the equations and get $N_A = 65.84 \text{N}$, and $N_B = 0.16 \text{N}$, which are both positive number. Therefore, the whole system will not tip over at position 1.

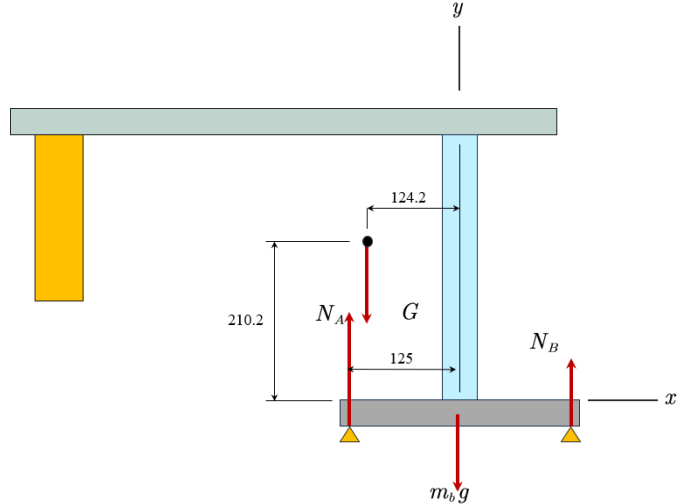


Fig. 22: Free body diagram of the whole system at position 1 (90°).

2) *Position 2:* When the cantilever is turned to 180° position, the free body diagram is shown in Fig. 23. Apply

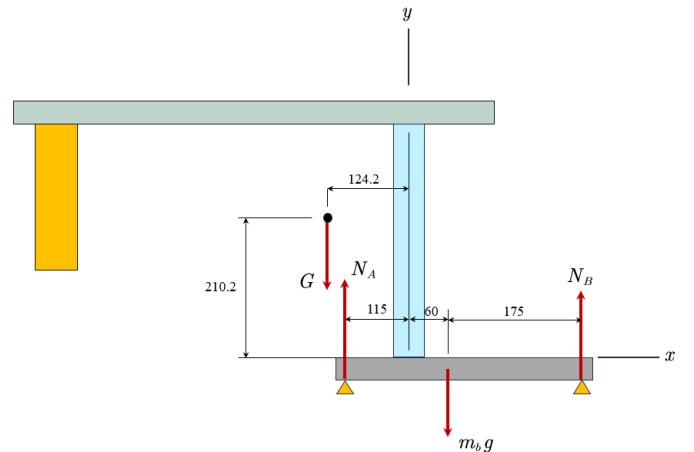


Fig. 23: Free body diagram of the whole system at position 2 (180°).

equilibrium equations, we have

$$\begin{aligned} \sum F_y &= N_A + N_B - 51 - 15 = 0 \\ \sum M_A &= 51 \times (124.2 - 115) + N_B \times 350 - 15 \times 175 = 0 \end{aligned}$$

Solve the equations and get $N_A = 59.84 \text{N}$, and $N_B = 6.16 \text{N}$, which are both positive numbers. Therefore, the whole system will not tip over at position 2.

With the above analysis, we can assure that the system will balance at whatever position. The design of the mass distribution is therefore justified.

V. DEMONSTRATION OF THE DEVICE

After completing the assembly of the device, we verified the degrees of freedom in four dimensions and tested its capability of gripping different objects. The results are shown as follows.

A. Gripping Capability

The first target of the gripping test is an elastic ball with a diameter of 7 centimeters. The experimental evidence shows that the device can grasp the ball and control its movement in different directions, and the results meet our expectations.

The second target of the gripping test is an empty plastic bottle with a diameter of 6 centimeters and a height of 12 centimeters. The experimental evidence shows that the device can grasp the bottle and control its movement in different directions, and the results meet our expectations. All the details are shown in Fig. 24

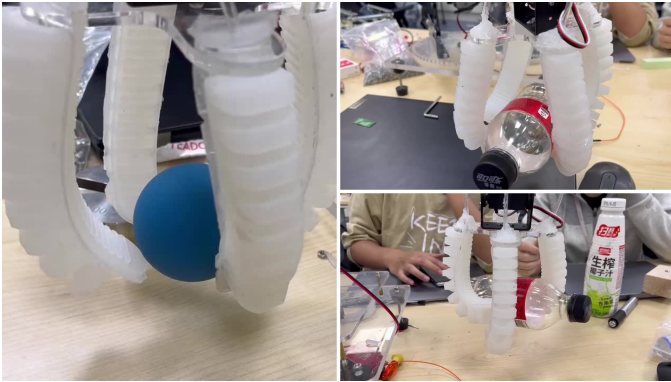


Fig. 24: Gripping test of an elastic ball and a plastic bottle.

The third target of the gripping test is a wooden ball with a diameter of 2 centimeters. The experimental evidence shows that the device is capable of grabbing the wooden ball, moving it in three directions, and finally releasing it in the designated position. The experimental results meet our expectations.

The fourth target of the gripping test is a ping-pong ball with a diameter of 4 centimeters. The experimental evidence shows that the device is capable of grabbing the ping-pong ball, moving it in three directions, and finally releasing it in the designated position. The experimental results meet our expectations. All the details are shown in Fig. 25

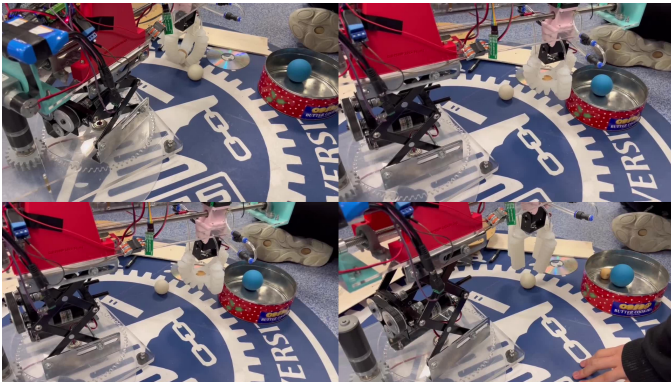


Fig. 25: Gripping test of a wooden ball and a ping-pong ball

B. Load caring capacity

Through test and analysis of the device, we find that it can move on four designated degrees of freedom, which confirms

that our design and material selection can meet functional requirements.

The test results prove that the device can rotate freely in the horizontal direction. The details are shown in Fig. 26



Fig. 26: Free horizontal rotation of the device

The test results prove that the gripper can move freely in the horizontal direction. The details are shown in Fig. 27



Fig. 27: Free horizontal movement of the gripper

The test results prove that the device can move freely in the vertical direction. The details are shown in Fig. 28

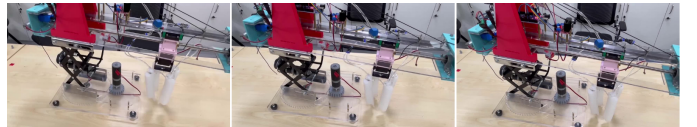


Fig. 28: Free vertical movement of the device

The test results prove that the gripper can rotate freely with the axis of the robot arm. The details are shown in Fig. 29

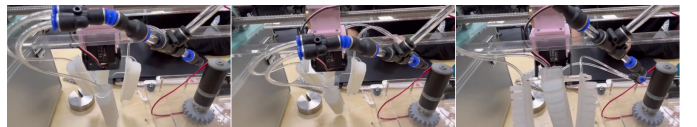


Fig. 29: Free vertical rotation of the gripper

VI. CONTROL AND CIRCUIT

The whole system is controlled by an Arduino Mega 2560 Rev3 microcontroller based on ATmega2560 [15]. To remotely control every part of the robotic arm and the soft gripper, we use the HC-02 Bluetooth module [16] to realize the communication between an Android phone and the Arduino board.

A. Arduino Code and Flowchart

The entire Arduino code is provided in Appendix D. The main part of the control code is that it runs in an endless loop, in which it hears from the Bluetooth module the command the user has sent (details in the next section). After it receives a command, which is represented by a single char, it will perform the corresponding operation by sending signals to various electronic components like a motor, air pump, or solenoid valve.

The flowchart of the code is shown in Fig. 30. When the device starts, it begins by setting up the communication with the HC-02 Bluetooth module over serial ports. It attaches a servo motor to a designated pin and sets its initial position to a specific angle (neutral position). It then prints a welcome message on the serial monitor. The code then defines several pins to control the different motors as OUTPUT, which means these pins will be used to send signals to the motors. All motors and a relay are turned off initially to prevent any unintentional movements when the device is powered up. The main part of the code runs in an endless loop, constantly checking for new input commands. If a command is received via one of the serial ports (Serial3), the code reads the character sent by the user. After reading an input character, the code prints the character to the serial monitor and checks the current position of the servo. Depending on the character received, the code performs different actions:

- Turn a bottom plate motor clockwise or counter-clockwise.
- Move a horizontal platform motor inward or outward.
- Move a vertical platform motor up or down.
- Operate a pump motor to either open the pump or close it.
- Activate a relay that controls the release of a gas.
- Rotate the servo motor clockwise or counter-clockwise to specific limits. It does this slowly, moving one degree at a time and pausing if new input is detected.

If a specific character (the '0' character) is received, the code turns off all motors and the relay, putting the machine into an idle state. The loop structure allows the device to be responsive at all times, acting on each new command as it comes in.

B. Design of Mobile Phone Application

To achieve the function of remote control through Bluetooth, a mobile phone application was designed with the help of the MIT app inventor. The UI of our mobile phone is shown in Fig. 31.

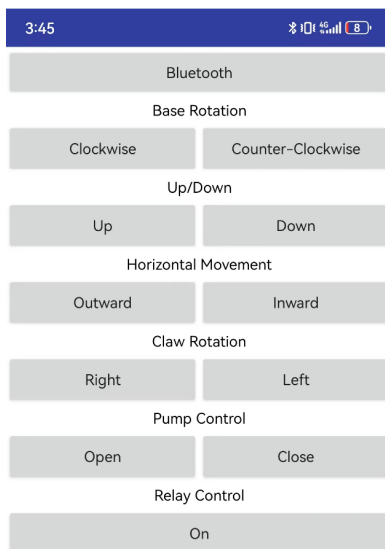


Fig. 31: The user interface of the mobile phone application. A total of 11 buttons control all 5 kinds of motion.

The mobile phone app is used to control the machine. By pushing down the button of the app, it will send a specific character to the HC-02 Bluetooth module, which is then used to control the corresponding activities of the motors and the relay. When the button is released, a '0' character will be sent, so that the current motion of the motors will be stopped.

The app can control the machine to perform the actions mentioned in the part above. In total, 11 buttons perform the following actions:

- Turn the base clockwise or counterclockwise.
- Turn the base counter-clockwise.
- Lifting arm.
- Lowering arm.
- Move the claw outward.
- Move the claw inward.
- Rotate the claw motor clockwise.
- Rotate the claw motor counter-clockwise.
- Open the pump motor.
- Close the pump motor.
- Activate the relay to release gas in the gripper.

We can simply click the button to achieve the action. As mentioned before, when clicked, each button will generate and send a signal to the Bluetooth module. The signal is represented by a single char, and each button generates a different signal. The control module will control the machine to perform the corresponding operations.

Except for the 11 buttons, there is also a 'Bluetooth' list-picker. It is used to connect the mobile phone to the Bluetooth module on the machine. We first click it, and we will turn into a page that shows all Bluetooth devices neighboring the mobile phone. Then, select the HC-02 Bluetooth module. When the LED light of the Bluetooth module is always on, it means that the connection is successful.

C. Electrical Components and Circuit Diagram

The circuit block diagram is shown in Fig. 32, and the wire connection between each component is illustrated in Fig. 33. We use a DC 12V battery to power the whole system because all the DC motors work at this voltage. The 12v battery will power the Arduino Mega, the motor parts of two BTS7960 motor drivers, and the solenoid valve. Then, a 5-volt voltage is taken out of the Arduino Mega board to power the HC-02 Bluetooth module, the signal part of two BTS7960 motor drivers, the servo motor, and the relay.

1) The Solenoid Valve and Relay: The solenoid valve is used to balance the air pressure in and outside the gripper's air chamber, so as to make the gripper soft when it is supposed to put items down. The relay serves as a digital switch. When there is a HIGH signal at the relay, it will open the solenoid valve, which will cause air to flow out from the soft gripper.

2) The Bluetooth Module: In this project, we want to realize the function that the whole system is controlled by a mobile phone application. The media for this wireless communication is the HC-02 Bluetooth module. This module communicates with the Arduino Mega through UART. Each time the user presses or releases a button on the mobile phone application, one character will be sent to the Arduino by HC-02 as

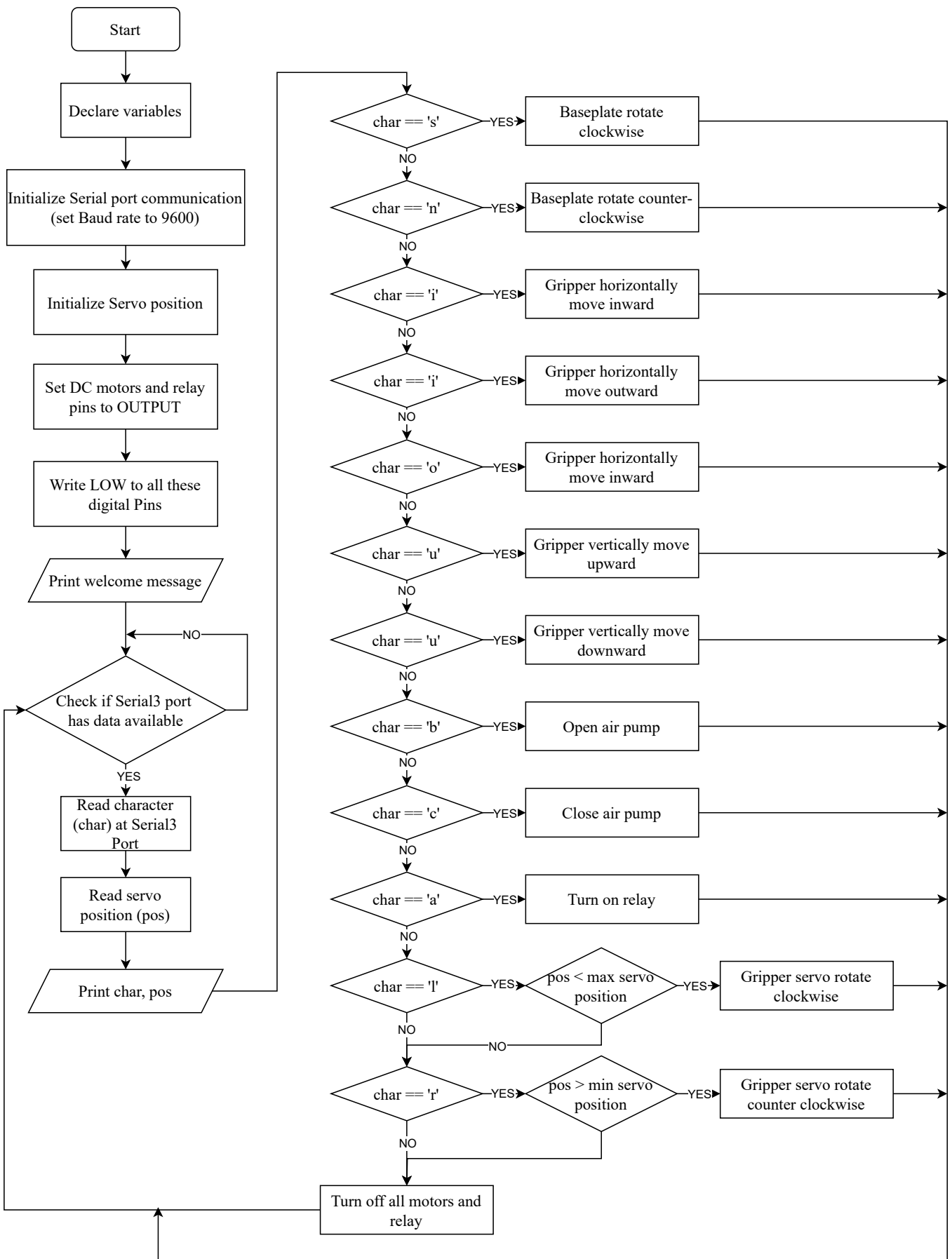


Fig. 30: The flowchart of Arduino code

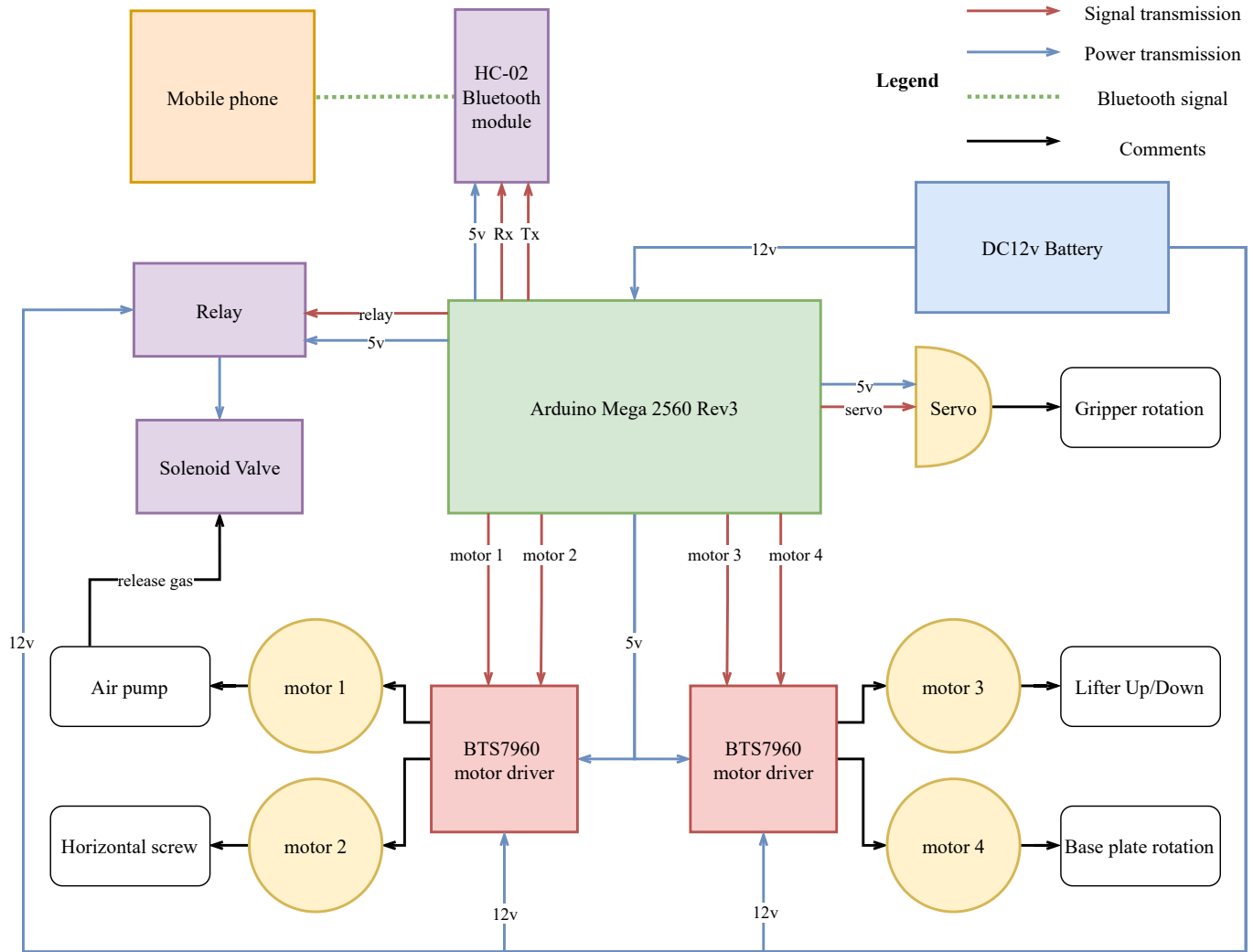


Fig. 32: The circuit block diagram of the whole system. As shown in the *Legend*, the blue arrow shows the power transmission, the red arrows show the signal transmission, the green dashed line represents the communication between the mobile phone and the Bluetooth module, and the black arrows are mainly used to illustrate some comments on the function of the electronic components.

char type. The code will process this character and make further decisions on other electrical components. The reason we choose HC-02 as the media for communication is that it is easy to use, cheap, and widely adaptable to Android, IOS, and other systems.

VII. DISCUSSION

A. Differences between Theoretical Analysis and Test Results

From the theoretical analysis and demonstration tests, we have found the following agreements and disagreements in terms of design effectiveness, system stability, material appropriateness, and grasping performance.

1) *Design effectiveness:* Our proposed work aims to design a robotic arm system with a soft gripper to accomplish grasping and manipulation tasks. Through testing, the crane-like arm system can effectively realize motions in four degrees of freedom with Bluetooth control. Meanwhile, the pneumatic

gripper with four fingers can successfully perform bending and relaxing with the control of air pump. Tests have shown the gripper's capability of grasping balls of different materials and sizes in different configurations and manipulating water bottles to complete pouring tasks. Therefore, our design is effective.

2) *System stability:* Our theoretical framework for system stability was rigorously tested through a combination of static analysis, finite element analysis, and mass center calculation, providing a solid foundation for the physical construction of the soft pneumatic gripper system.

In terms of static analysis, we calculated the forces and moments acting on the system in the equilibrium state. We therefore deduced the necessary thickness of the acrylic board for the cantilever's bottom board, ensuring a safety factor of 3 was maintained. Simultaneously, the FEA served as a critical validation tool, with Solidworks simulations confirming our theoretical stress and deflection calculations. The simulation results indicated a maximum von Mises stress that was safely

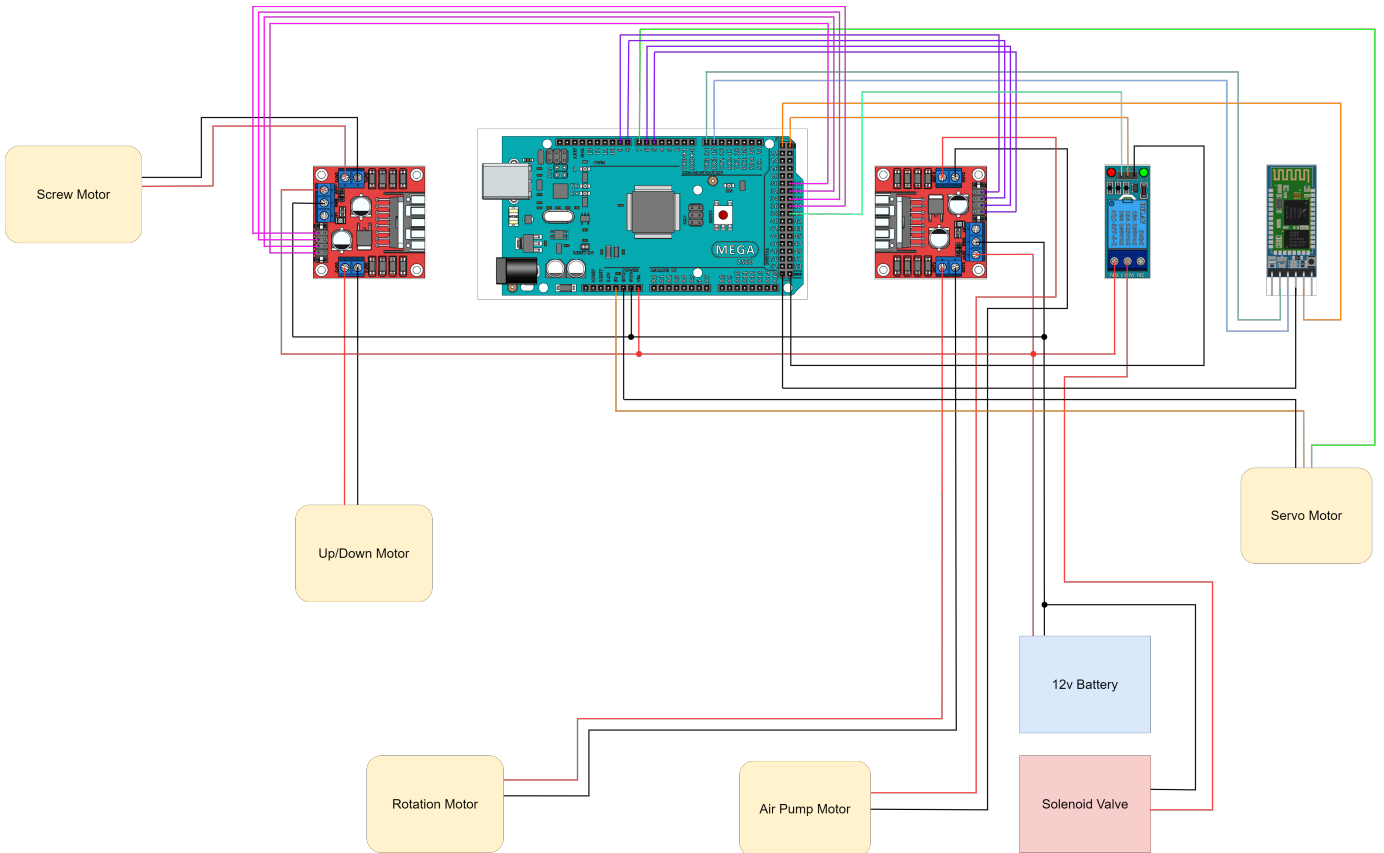


Fig. 33: The wire connection between each electrical component. Notice that some electrical components are not labeled with a name, but rather with a picture of the component. The placement of each component, to some extent, represents the actual place where each component is fixed to the machine.

below the material yield stress, thus corroborating the adequacy of the 4mm thickness for the acrylic board.

However, disagreements still exist. In our case, the FEA also highlighted the significant deflection at the cantilever's tip, which was not as pronounced in our initial theoretical models. This insight led to the practical implementation of balancing ropes to counteract excessive deflection, demonstrating the iterative nature of design and the importance of adapting theoretical models in light of practical observations.

The analysis of the system's mass center and its balance during rotational movements was another area where theoretical calculations were successfully mirrored by real-world behavior. The calculations predicted that the system would remain stable during rotations, even at its most extended and vulnerable positions, which was affirmed during physical testing.

3) Material appropriateness: The material selection process for the robotic arm and soft gripper was underpinned by theoretical predictions, leveraging Ashby charts to identify optimal candidates based on mechanical properties. PMMA was chosen for the cantilever panels to balance lightness and stiffness, while aluminum alloy was selected for the X-shaped lifter's scissor rods due to its favorable stiffness-to-weight ratio. However, due to the difficulty of real-life practice, some compromises have to be made. For example, while the aluminum alloy is the best candidate for the cantilever

panel with minimum weight and maximum strength, we have to choose PMMA as the material for the convenience of manufacturing. Therefore, our final system is heavier than we expected.

4) Tolerance control: One aspect that the reality fails to align with theoretical analysis is about tolerance control of bearings and the base plate. The bearing arrangement was designed to ensure a secure connection between the upper half of the arm and the base. The rotation structure involved using bearings inserted into holes: one in the center of the gear (part of the upper half) and another in the base. These bearings were then linked by a shaft, effectively joining the top half and the base.

The theoretical expectation was that the bearing fit would be either a line fit or even an interference fit, creating a tight connection. The goal was to achieve a robust and stable structure that could withstand mechanical stresses during operation.

Unfortunately, during testing, the top half of the robotic arm fell over. The critical issue was that the hole in the center of the gear became detached from the bearing with which it was combined. This unexpected failure indicates a significant discrepancy between the theoretical analysis and the actual performance. We think that the root cause lies in the lack of proper tolerance control during manufacturing and assembly. Specifically, the bearing fit was not precisely aligned with the theoretical expectations. Without the desired tight fit, the entire

structure lacked stability, leading to the top half toppling over.

To address this issue, we think out several ways:

- **Tolerance verification:** Ensure that the actual bearing dimensions match the design specifications. Regular inspections during manufacturing can prevent deviations.
- **Material Properties:** Consider the material properties of the bearing and the surrounding components. Different materials may expand or contract differently under load or temperature changes.
- **Assembly Procedures:** Implement precise assembly procedures to achieve the desired fit. Proper alignment and secure attachment are crucial.
- **Iterative Design:** Use the test results to refine the design iteratively. Adjust tolerances, material choices, and assembly techniques based on empirical data.

B. Intellectual Merit

This work holds significant intellectual merit through its innovative contribution to soft robotics, showcasing a design that adeptly handles a spectrum of object shapes and sizes. The integration of a soft pneumatic gripper with a sophisticated control system within a crane-like robotic arm presents an interdisciplinary achievement, merging mechanical design, material properties, and computational control. Theoretical analysis and empirical testing reinforce the system's robustness, while the wireless control via a mobile application introduces a new dimension in user interaction.

C. Implications

Our comprehensive theoretical analysis and tests lead to both theoretical and practical implications.

The theoretical implications of this work are significant, offering a substantial contribution to the field of soft robotics. The innovative design of the soft pneumatic gripper, with its adaptive grasping capabilities, presents a new theoretical model for robotic manipulation of complex geometries. The independent actuation of each gripper finger and the integration with a crane-like robotic arm introduce novel concepts in mechatronic system design, expanding the scope of control strategies and user interactions. The rigorous static analysis and empirical testing underpin a robust theoretical framework for safety and functionality, setting a precedent for future soft robotic systems. Material selection justified through Ashby charts and the detailed manufacturing process provide a methodological approach that can be generalized to other robotic designs. Collectively, these theoretical advancements lay the groundwork for the development of sophisticated soft robotic devices for a wide array of applications, from medical to rescue operations, thereby influencing the trajectory of future research and technological innovation in the field.

Although our soft gripper system does not exactly yield all expected results and performance, it still leads to a wide range of applications in various fields, including biology, medical, and disaster rescue. In terms of biology, our proposed soft gripper could be used to sample deep reefs in the ocean, or it could be used in other water environments where delicate manipulations on soft or fragile organisms are required [17].

In addition, soft grippers allow for safer clinical interactions with human patients. [18] Therefore, combined with our control system, our soft grippers have the potential to be used in minimally invasive surgery, helping rehabilitation and functioning as assistance devices. Finally, the flexibility of the soft gripper and the large range of movement of the control system enables our work to be implemented in disaster rescue. For example, after an earthquake, our crane with the soft gripper could be used to help carry out the victims from the ruins without hurting them, therefore improving the rescue efficiency and lowering the death rate. With so many possible and meaningful applications, our work holds considerable practical significance.

VIII. CONCLUSION

This study aims to design, manufacture, and control a soft pneumatic gripper in a crane-like system to complete different grasping and manipulation tasks, looking for potential applications in broader fields. The whole control system has four degrees of freedom, allowing the soft gripper to grasp objects with varying shapes and sizes. Specifically, the system and the gripper can have radial, axial, longitudinal, and rotational motions, which are empowered by the motors under the control of an Arduino circuit through a wireless terminal device. The pneumatic soft gripper adopts the design of independent FEAs, whose exerting force comes from the bending transformation caused by the air pressure in the cells. Through a comprehensive theoretical analysis that justifies the feasibility of the system and several tests that directly show its effectiveness, we have the following key findings:

- 1) **Adaptable Gripping Mechanism:** The soft pneumatic gripper is capable of grasping a variety of objects with different shapes and sizes, highlighting its adaptability.
- 2) **Integrated Control System:** The soft gripper, when combined with a robotic arm featuring four degrees of freedom, enables precise manipulation tasks.
- 3) **Independent FEA Design:** The use of independent Fluidic Elastomer Actuators (FEAs) in the gripper design allows for controlled and variable grasping forces.
- 4) **Wireless Operation:** The custom mobile app and Bluetooth module provide a convenient and efficient wireless control scheme for the system.
- 5) **Validated Stability and Safety:** The system's stability and safety have been confirmed through rigorous theoretical analysis and empirical testing.

Future studies could focus on the improvement of the control system, such that the gripper fingers could be independently controlled, allowing for more adaptability and user-friendly control. Meanwhile, it remains to see whether the configuration of the gripper fingers could be improved so that it can grasp objects more effectively. The manufacturing process of the grippers could also be standardized with more advanced machines to ensure consistency between the gripper fingers.

In conclusion, this project successfully developed a soft pneumatic gripper integrated into a crane-like robotic system, showcasing its potential for versatile applications across various fields. The project's findings not only contribute to the

field of soft robotics but also pave the way for future advancements in control systems, gripper finger configurations, and manufacturing processes.

REFERENCES

- [1] S. Kim, C. Laschi, and B. Trimmer, "Soft robotics: A bioinspired evolution in robotics," *Trends in biotechnology*, vol. 31, 04 2013.
- [2] J. F. Elfferich, D. Dodou, and C. Della Santina, "Soft robotic grippers for crop handling or harvesting: A review," *IEEE Access*, vol. 10, pp. 75 428–75 443, 2022.
- [3] J. Shintake, V. Cacucciolo, D. Floreano, and H. Shea, "Soft robotic grippers," *Advanced Materials*, vol. 30, no. 29, p. 1707035, 2018. [Online]. Available: <https://onlinelibrary.wiley.com/doi/abs/10.1002/adma.201707035>
- [4] K. C. Galloway, K. P. Becker, B. Phillips, J. Kirby, S. Licht, D. Tchernov, R. J. Wood, and D. F. Gruber, "Soft robotic grippers for biological sampling on deep reefs," *Soft robotics*, vol. 3, no. 1, pp. 23–33, 2016.
- [5] G. M. Whitesides, "Soft robotics," *Angewandte Chemie International Edition*, vol. 57, no. 16, pp. 4258–4273, 2018. [Online]. Available: <https://onlinelibrary.wiley.com/doi/abs/10.1002/anie.201800907>
- [6] Z. Kan, C. Pang, Y. Zhang, Y. Yang, and M. Y. Wang, "Soft actuator with programmable design: Modeling, prototyping, and applications," *Soft Robotics*, vol. 9, no. 5, pp. 907–925, 2022.
- [7] E. Brown, N. Rodenberg, J. Amend, A. Mozeika, E. Steltz, M. R. Zakin, H. Lipson, and H. M. Jaeger, "Universal robotic gripper based on the jamming of granular material," *Proceedings of the National Academy of Sciences*, vol. 107, no. 44, pp. 18 809–18 814, 2010.
- [8] Z. Wang, P. Polygerinos, J. T. Overvelde, K. C. Galloway, K. Bertoldi, and C. J. Walsh, "Interaction forces of soft fiber reinforced bending actuators," *IEEE/ASME Transactions on Mechatronics*, vol. 22, no. 2, pp. 717–727, 2016.
- [9] B. Gorissen, D. Reynaerts, S. Konishi, K. Yoshida, J.-W. Kim, and M. De Volder, "Elastic inflatable actuators for soft robotic applications," *Advanced Materials*, vol. 29, no. 43, p. 1604977, 2017.
- [10] P. Polygerinos, N. Correll, S. A. Morin, B. Mosadegh, C. D. Onal, K. Petersen, M. Cianchetti, M. T. Tolley, and R. F. Shepherd, "Soft robotics: Review of fluid-driven intrinsically soft devices; manufacturing, sensing, control, and applications in human-robot interaction," *Advanced Engineering Materials*, vol. 19, no. 12, p. 1700016, 2017.
- [11] F. Ilievski, A. D. Mazzeo, R. F. Shepherd, X. Chen, and G. M. Whitesides, "Soft robotics for chemists," *Angewandte Chemie International Edition*, 2011.
- [12] B. Mosadegh, P. Polygerinos, C. Keplinger, S. Wennstedt, R. F. Shepherd, U. Gupta, J. Shim, K. Bertoldi, C. J. Walsh, and G. M. Whitesides, "Pneumatic networks for soft robotics that actuate rapidly," *Advanced functional materials*, vol. 24, no. 15, pp. 2163–2170, 2014.
- [13] Y. Hao, Z. Gong, Z. Xie, S. Guan, X. Yang, Z. Ren, T. Wang, and L. Wen, "Universal soft pneumatic robotic gripper with variable effective length," in *2016 35th Chinese Control Conference (CCC)*, 2016, pp. 6109–6114.
- [14] M. F. Ashby, *Materials selection in mechanical design*. Butterworth-Heinemann, 2017.
- [15] Arduino, "Mega 2560 rev3," <https://docs.arduino.cc/hardware/mega-2560/>, Arduino, 2023, [Online; accessed 04-20-2024].
- [16] HuiCheng, "Hc-02 bluetooth 4.0 ble slave module to uart transceiver for arduino compatible with android and ios osoyoo.com." [Online]. Available: <https://osoyoo.com/2018/07/13/hc-02-bluetooth-4-0-ble-slave-module-to-uart-transceiver-arduino-compatible-with-android-ios/>
- [17] K. C. Galloway, K. P. Becker, B. Phillips, J. Kirby, S. Licht, D. Tchernov, R. J. Wood, and D. F. Gruber, "Soft robotic grippers for biological sampling on deep reefs," *Soft Robotics*, vol. 3, no. 1, pp. 23–33, 2016, PMID: 27625917. [Online]. Available: <https://doi.org/10.1089/soro.2015.0019>
- [18] J.-H. Hsiao, J.-Y. Chang, and C.-M. Cheng, "Soft medical robotics: clinical and biomedical applications, challenges, and future directions," *Advanced Robotics*, vol. 33, no. 21, pp. 1099–1111, 2019.

APPENDIX A CONTRIBUTION OF THE TEAM MEMBER



Guanyu Xu Grouper leader. Mainly responsible for mechanical design of robotic arm and soft gripper, as well as the programming of Arduino code. Assist writing the technical report and design review presentation.



Jiawen Li Group manager. Responsible for project management and technical communication, including the design review presentation and final report. Actively participated in brainstorming, assembly, and testing process.



Weixuan Zhang Group member. Responsible for the gripper manufacturing, mobile app programming and the controlling of the machine. Also participated in fabrication, testing and tuning process.



Youle Chen Responsible for technical issues, including manufacturing of components and modeling of grippers. Actively participate in brainstorming, assembly and testing process.

APPENDIX B GANTT CHART

The Gantt chart of our group is shown in Fig. 34. We spent about seven weeks in completing the whole project. All tasks are evenly distributed to each team members, and we complete them on schedule.

APPENDIX C BUDGET TABLE AND JUSTIFICATION

The budget table is presented in Table IV. The total budget of our project is ¥789.66, which is within the budget limit.

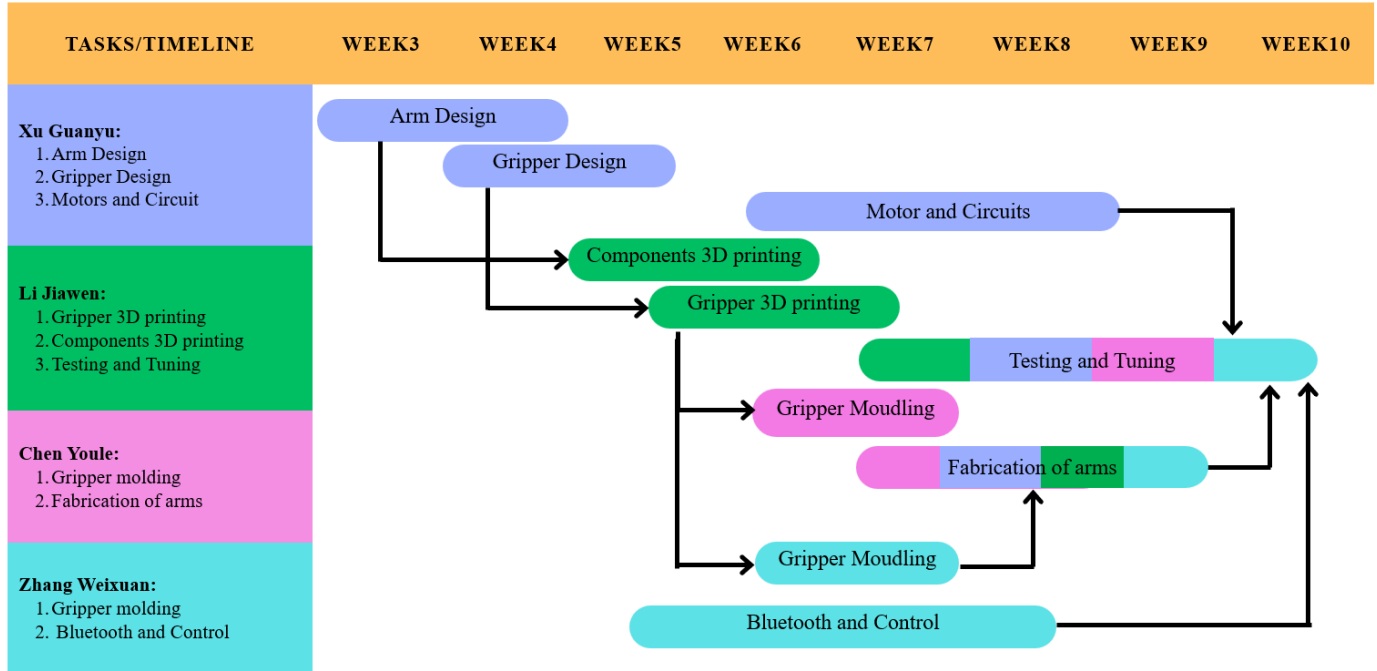


Fig. 34: The Gantt chart

TABLE IV: The budget table. In this table, total price is the sum of *Number* times *Unit Price* of all items, and total budget refers to the extra item we bought in this project. The items with a (*) in the *Name* column does not count in the total budget.

Category	Name	Details	Number	Unit Price
Gripper	Vacuum Air Pump (*)	ES-3910, DC12V	1	¥28.50
	Solenoid Valve (*)	2V025-08, DC12V	1	¥27.00
	Air Tube Connector	PE-8, PY-4, PG8-4, PC8-02	1	¥10.37
	Servo Motor	Double Axis, 10Kg, DC6V	1	¥39.90
Horizontal Movement	Linear Screw	10mm*600mm	1	¥39.50
	Linear Track	HGR15-100mm	5	¥3.70
	Sliding Block	HGW15CC	1	¥15.00
	Screw Motor	4632-370, DC12V, 150RPM	1	¥27.00
Vertical Movement	X-shaped Lifter	150mm*150mm	1	¥420.00
	Lifter Motor	36GM-36ZY, DC12V, 570RPM	1	¥85.00
Base Rotation	Base Rotation Motor	36GM-3530, DC12V, 1540RPM	1	¥49.00
	Motor Flange	D-shape axis, 8mm	1	¥3.36
	Bearing	10*30*9mm	2	¥1.30
	Connecting Shaft	10*20mm	1	¥0.42
Control	Arduino Microcontroller (*)	MEGA 2560 R3	1	¥70.00
	Bluetooth module (*)	HC-02	1	¥13.50
	Motor Driver (*)	BTS7960	4	¥11.50
	Lithium-ion Battery	DC12V, 2800mAh	1	¥44.50
	Motor Wire (*)	2*0.3 square meter, 10m	1	¥11.00
				Total Price: ¥951.15
				Total Budget: ¥789.66

APPENDIX D ARDUINO PROGRAMMING CODE

```

1 #include <SoftwareSerial.h>
2 #include <Servo.h>
3
4 //base plate rotation motor
5 const int RMotor_RPWM = 8;
6 const int RMotor_LPWM = 9;
7 const int RMotor_REN = 30;
8 const int RMotor_LEN = 31;
9 //X-shape lifter motor
10 const int LMotor_RPWM = 11;
11 const int LMotor_LPWM = 10;
12 const int LMotor_REN = 29;
13 const int LMotor_LEN = 28;
14 //Cantilever screw motor
15 const int SMotor_RPWM = 5;
16 const int SMotor_LPWM = 4;
17 const int SMotor_REN = 35;
18 const int SMotor_LEN = 34;
19 //Pump motor (PMotor)
20 const int PMotor_RPWM = 6;
21 const int PMotor_LPWM = 7;
22 const int PMotor_REN = 32;
23 const int PMotor_LEN = 33;
24 //Relay signal pin
25 const int Relay = 36;
26 //Servo signal pin
27 const int servoPin = 12;
28 Servo myServo;
29 char input;
30 int pos;
31 void setup()

```

```

32  {
33   Serial.begin(9600);
34   Serial3.begin(9600);
35   myServo.attach(servoPin);
36   //initialize servo position
37   myServo.write(115);
38   Serial.println("Welcome to VM250 Project!");
39   for (int i = 4; i <= 11; i++)
40   {
41     pinMode(i,OUTPUT);
42     digitalWrite(i,0);
43   }
44   for (int i = 28; i <= 35; i++)
45   {
46     pinMode(i,OUTPUT);
47     digitalWrite(i,HIGH);
48   }
49   pinMode(Relay,OUTPUT);
50   digitalWrite(Relay,LOW);
51 }
52 void loop()
53 {
54   if (Serial3.available() > 0)
55   {
56     input = Serial3.read();
57     Serial.print("Char received:");
58     Serial.println(input);
59     pos = myServo.read();
60     Serial.print("The Position of the servo:");
61     Serial.println(pos);

63     if (input == 's')
64     //Bottom plate turn clockwise
65     {
66       analogWrite(RMotor_RPWM,255);
67       analogWrite(RMotor_LPWM,0);
68     }
69     if (input == 'n')
70     //Bottom plate turn counter-clockwise
71     {
72       analogWrite(RMotor_RPWM,0);
73       analogWrite(RMotor_LPWM,255);
74     }
75     if (input == 'i')
76     //Horizontal move inward
77     {
78       analogWrite(SMotor_RPWM,0);
79       analogWrite(SMotor_LPWM,255);
80     }
81     else if (input == 'o')
82     //Horizontal move outward
83     {
84       analogWrite(SMotor_RPWM,255);
85       analogWrite(SMotor_LPWM,0);
86     }
87     if (input == 'u')
88     //Platform move up
89     {
90       analogWrite(LMotor_RPWM,0);
91       analogWrite(LMotor_LPWM,255);
92     }
93     else if (input == 'd')
94     //Platform move down
95     {
96       analogWrite(LMotor_RPWM,255);
97       analogWrite(LMotor_LPWM,0);
98     }
99     else if (input == 'b')
100    //open the pump
101    {
102      analogWrite(PMotor_RPWM,0);
103      analogWrite(PMotor_LPWM,255);
104    }
105    else if (input == 'a')
106    //release gas
107    {
108      digitalWrite(Relay,HIGH);
109    }
110  }
111  else if (input == 'c')
112  //close the pump
113  {
114    analogWrite(PMotor_RPWM,0);
115    analogWrite(PMotor_LPWM,0);
116  }
117  else if (input == 'l')
118  // Servo rotate clockwise
119  {
120    while (pos < 160)
121    {
122      myServo.write(pos + 1);
123      pos = myServo.read();
124      delay(10);
125      if (Serial3.available())
126      {
127        input = Serial3.read();
128        Serial.println(input);
129        break;
130      }
131    }
132    else if (input == 'r')
133    //Servo rotate counter clockwise
134    {
135      while (pos > 20)
136      {
137        myServo.write(pos - 1);
138        pos = myServo.read();
139        delay(10);
140        if (Serial3.available() > 0)
141        {
142          input = Serial3.read();
143          Serial.println(input);
144          break;
145        }
146      }
147    }
148  }
149  else if (input == '0')
150  {
151    analogWrite(RMotor_RPWM,0);
152    analogWrite(RMotor_LPWM,0);
153    analogWrite(LMotor_RPWM,0);
154    analogWrite(LMotor_LPWM,0);
155    analogWrite(SMotor_RPWM,0);
156    analogWrite(SMotor_LPWM,0);
157    digitalWrite(Relay,LOW);
158  }
159 }
160 }
```

APPENDIX E VIDEO LINK

If you are interested, here is a link for the project video which demonstrates the basic functions and records the manufacturing process of the system: <https://www.bilibili.com/video/BV1rZ421J7Z6>.

ACKNOWLEDGMENT

The authors would like to thank the help of Professor Ju Jaehyung and all the TAs. In addition, we would like to thank the help from all our classmates and friends in ME250. Never will we forget the spring with you.